

A Graph Signal Processing Framework for Atrial Activity Extraction

Miao Sun*, Elvin Isufi*, Natasja M.S. de Groot[†], and Richard C. Hendriks*

*Circuits and Systems (CAS) Group, Delft University of Technology, The Netherlands

[†]Department of Cardiology, Erasmus University Medical Center, The Netherlands

E-mails: * {m.sun, e.isufi-1, r.c.hendriks}@tudelft.nl, [†]n.m.s.degroot@erasmusmc.nl

Abstract—Atrial fibrillation (AF) is a common cardiac arrhythmia and its mechanisms are not yet fully understood. Analyzing atrial epicardial electrograms (EGMs) is important to understand the mechanisms underlying AF. However, when measuring the atrial activity (AA), the electrogram is commonly distorted by the far-field ventricular activity (VA). During sinus rhythm, the AA and the VA are separated in time. However, the VA often overlaps with the AA in both time and frequency domain during AF, complicating proper analysis of the AA. Unlike traditional methods, this work explores graph signal processing (GSP) tools for AA extraction in EGMs. Since EGMs are time-varying and non-stationary, we put forward the joint graph and short-time Fourier transform to analyze the graph signal along both time and vertices. It is found that the temporal frequency components of the AA and the VA exhibit different levels of spatial variation over the graph in the joint domain. Subsequently, we exploit these findings to propose a novel algorithm for extracting the AA based on graph smoothness. Experimental results on synthetic and real data show that the smoothness analysis of the EGMs over the atrial area enables us to better extract the AA.

Index Terms—Atrial fibrillation, atrial activity extraction, graph-time signal processing, graph smoothness.

I. INTRODUCTION

Atrial fibrillation (AF) is a common heart disease characterized by rapid and irregular beating of the atria. Its prevalence among the general population is about 1% - 2%, which is predicted to double in the next 50 years [1]. The mechanisms of AF are complicated and not clear yet. Compared to body surface electrocardiograms (ECGs), epicardial electrograms (EGMs) are measured on the heart surface and have a better spatial resolution, which is helpful to investigate the mechanisms underlying AF. Therefore, we focus on the EGMs in this work. Atrial EGMs are usually corrupted by ventricular far-field activity. Although ventricular activity (VA) and atrial activity (AA) are separated in time during sinus rhythm, they overlap during AF. This complicates the analysis of AF and emphasizes why it is important to remove VA from the raw measurements before using electrograms for studying activation patterns during AF.

One commonly applied technique to extract AA is called template matching and subtraction [2]–[4], which generates a template of the VA and then subtracts it from the raw measurements. Average beat subtraction (ABS) [2] is a simple but effective implementation of this technique. However, it

cannot adapt well to changes in the morphology of the electrogram. Another technique, called adaptive ventricular cancellation (AVC) [5], is proposed to solve this problem. However, its performance is not stable as it depends on a reference recording, usually obtained from another lead. For surface ECG, signal separation algorithms such as principal component analysis (PCA) [6] and independent component analysis (ICA) [5], [7] are also explored for AA extraction. However, the assumptions about the distribution and independence of the ECG components may not hold for the EGM.

The EGMs considered in this work are measured at the epicardial sites of the atria by a mapping array. These data are spatially high dimensional and exhibit irregular properties during AF. The natural tools to represent such data are graphs, as graphs have proven their ability to capture the underlying structure of high-dimensional and irregular data [8]. Therefore, we construct an undirected graph to represent the EGMs in all electrodes and then analyze the spatial variation of the AA and the VA using tools from graph signal processing (GSP) [8], [9].

The graph Fourier transform (GFT) is a predominant tool in GSP, which permits to decompose a graph signal (in our case the EGM measurements) into components that exhibit different levels of spatial variation. However, it only considers a fixed time sample and cannot exploit the correlation in time. Considering that EGMs are time-varying and non-stationary, we use the short-time Fourier transform (STFT) in combination with the GFT to exploit the spatial variation of the AA and the VA in short time periods. In the joint space-time-frequency domain it is found that the frequency components of the VA are less variable over the atrial area than those of the AA. This motivates us to separate the AA and the VA based on their difference in smoothness over the graph. In this regard, we develop an algorithm to extract the AA based on the graph smoothness.

II. PROBLEM STATEMENT

The data used in this study are obtained from [10] and are measured during open-heart surgery at Bachmann’s bundle using a high-resolution mapping array, as shown in Fig. 1, during both sinus rhythm (SR) and induced AF. All procedures performed in the data collection were in accordance with the ethical standards as declared in [10]. There are 8×24 electrodes in the array with an inter-electrode distance of 2

M. Sun’s work is supported by the Oversea Study Program of Guangzhou Elite Project.

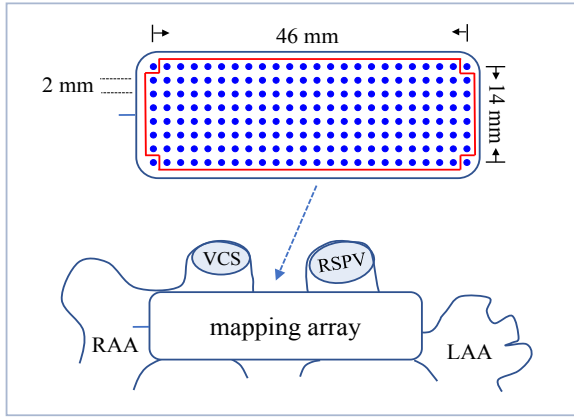


Fig. 1. The mapping array and the placement on Bachmann's bundle (BB) in a human heart [10]. RAA: right atrial appendage; LAA: left atrial appendage; VCS: vena cava superior; RSPV: right superior pulmonary vein.

mm. The electrodes included in the red box in Fig. 1 are used for recording the EGMs. One of the remaining electrodes is used to measure the ECG. Fig. 2 shows an example of the EGM during SR and during AF. We use red triangles to mark the peaks of the ventricular components, whose positions are determined using the ECG. From Fig. 2, we can see that the AA and the VA do not overlap during SR whereas they often overlap during AF. We here aim to extract the AA from the mixture, which is in particular challenging during AF due to the fact that the AA and the VA overlap in frequency as well as in time domain.

We treat each electrode as a vertex of a graph and connect it to its eight nearest neighbors to form an undirected network. Such a graph is reasonable as the signal at one electrode has strong similarities with the signals at surrounding electrodes. Denote the graph as $\mathcal{G} = (\mathcal{V}, \mathcal{E}, \mathbf{W})$, where $\mathcal{V} = \{v_1, \dots, v_m\}$ is the vertex set, \mathcal{E} is the edge set, and \mathbf{W} is the adjacency matrix collecting the edge weights $\mathbf{W}(i, j) = W_{i,j}$. We set $W_{i,j} = 1$ if there is a connection between vertices v_i and v_j and $W_{i,j} = 0$ if there is no connection. The graph signal is defined as a mapping from the vertex set to the set of real numbers. We denote the EGM in the i th electrode at time t as $x_{i,t}$. Then, $\mathbf{x}_t = [x_{1,t}, x_{2,t}, \dots, x_{m,t}]^\top \in \mathbb{R}^m$ with $t \in \{0, 1, \dots, T-1\}$ is the graph signal at time t .

We consider the EGM to be a linear mixture of the AA and the VA [5]. The EGM model can be expressed in the graph domain as

$$\mathbf{x}_t = \mathbf{a}_t + \mathbf{v}_t \quad (1)$$

where \mathbf{a}_t , \mathbf{v}_t , and \mathbf{x}_t represent the AA, the VA and the mixture on the graph, respectively.

To solve the AA extraction problem, we need to estimate the AA \mathbf{a}_t given the measurements \mathbf{x}_t . However, dealing with the graph signal per time sample neglects the time-domain correlation in the signal. Therefore, in this work, the AA is extracted in short-time periods by combining the joint short-time Fourier transform and the graph Fourier transform and

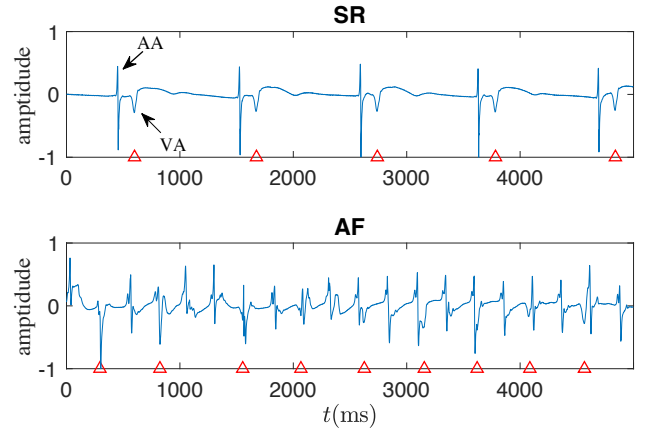


Fig. 2. An example of the EGM during SR and AF. The red triangles mark the time instants of the VA peaks.

by exploiting the graph signal smoothness in the joint space-time-frequency domain.

III. GRAPH SMOOTHNESS-BASED ATRIAL ACTIVITY EXTRACTION

In this section, we first introduce the basic GFT and then extend the transform from a fixed time sample to a short-time period by combining the STFT and GFT. Next, we compare the variation of the AA and the VA over the graph and introduce the AA extraction algorithm.

A. Graph Fourier Transform

Let $\mathbf{L} = \mathbf{D} - \mathbf{W}$ denote the graph Laplacian of an undirected graph, where \mathbf{D} is the diagonal degree matrix with $D_{i,i} = \sum_{j=1}^m W_{i,j}$. The Laplacian matrix \mathbf{L} is real and symmetric and accepts the eigenvalue decomposition $\mathbf{L} = \mathbf{U}\mathbf{\Lambda}\mathbf{U}^H$. Here, $\mathbf{\Lambda}$ is a diagonal matrix containing the eigenvalues λ_k ($k \in \{0, 1, \dots, m-1\}$) with increasing orders, $\mathbf{U} = [\mathbf{u}_0, \mathbf{u}_1, \dots, \mathbf{u}_{m-1}]$ is the set of orthonormal eigenvectors, and $(\cdot)^H$ is the Hermitian operator. We consider a graph signal $\mathbf{x}_t \in \mathbb{R}^m$ and a graph Laplacian operator \mathbf{L} . Then,

$$\tilde{\mathbf{x}}_t = \mathbf{U}^H \mathbf{x}_t \text{ and } \mathbf{x}_t = \mathbf{U} \tilde{\mathbf{x}}_t \quad (2)$$

define the GFT pair [9].

The GFT is a generalization of the traditional Fourier transform which decomposes the graph signal into components with different variation over the graph. The k th coefficient in $\tilde{\mathbf{x}}(t) = [\tilde{x}_{0,t}, \tilde{x}_{1,t}, \dots, \tilde{x}_{m-1,t}]^\top$ for low k indicates how much the slowly varying components contribute to the graph signal, whereas a larger k corresponds to the more rapidly varying components. Therefore, k is the graph frequency index. When $k = 0$, the GFT efficient $\tilde{x}_{0,t}$ indicates the contribution of the constant component to the signal. The smoothness of a signal over the graph can be measured using the graph Laplacian quadratic form [9]

$$S(\mathbf{x}_t) = \mathbf{x}_t^\top \mathbf{L} \mathbf{x}_t. \quad (3)$$

The value of $S(\mathbf{x}_t)$ is small if the signal has low variation over the graph, and it is large if the signal varies rapidly over the graph.

Nevertheless, the GFT just considers a fixed time instant and does not take the correlation across time of the graph signal into account. Therefore, it is less useful to analyze time-varying, correlated, and non-stationary signals such as the EGMs. In the following, the joint STFT and GFT is introduced for analyzing the time-varying graph signals in short-time periods.

B. Joint Graph and Short-time Fourier Transform

A classic method to analyze the spectrum of a non-stationary signal across time is the STFT, which transforms the data to the temporal frequency domain in short-time windows approximately satisfying stationarity. To analyze the non-stationary signals along both time and graph, we first apply the STFT to transform the signal at one vertex to the temporal frequency domain. Then, we are able to analyze the graph signal per temporal frequency per frame, as the STFT results in approximately decorrelated frequency components for each vertex.

The graph signals of all time instants are collected together in the matrix

$$\mathbf{X} = [\mathbf{x}_0, \mathbf{x}_1, \dots, \mathbf{x}_{T-1}] \in \mathbb{R}^{m \times T}. \quad (4)$$

The i th row of \mathbf{X} is the time-domain signal at the i th electrode. We apply the STFT to the i th row of \mathbf{X} to obtain the STFT coefficients for the i th electrode. The STFT coefficient in the temporal frequency bin f at the time-frame l is denoted as $\hat{x}_{i,l,f}$. Then, per time-frame l and frequency bin f , we stack the STFT coefficients of all vertices as $\hat{\mathbf{x}}_{l,f} = [\hat{x}_{0,l,f}, \hat{x}_{1,l,f}, \dots, \hat{x}_{m-1,l,f}]^T \in \mathbb{C}^m$. Applying then the GFT to $\hat{\mathbf{x}}_{l,f}$ as

$$\tilde{\mathbf{x}}_{l,f} = \mathbf{U}^H \hat{\mathbf{x}}_{l,f} \quad (5)$$

results in the joint STFT and GFT representation of the graph signal at temporal frequency bin f and time-frame l as $\tilde{\mathbf{x}}_{l,f} = [\tilde{x}_{0,l,f}, \tilde{x}_{1,l,f}, \dots, \tilde{x}_{m-1,l,f}]^T \in \mathbb{C}^m$. The coefficients $\tilde{x}_{k,l,f}$ for low values of k indicate now how much the slow varying components in the vertex domain contribute to the temporal frequency bin f at the l th time-frame.

To observe the contribution of different graph frequencies, we calculate the normalized signal energy per time-frame averaged over all temporal frequencies in the joint STFT and GFT domain as

$$E_{k,l} = 10 \log_{10} \left(\frac{1}{F_N} \sum_{f=0}^{F_N-1} \frac{|\tilde{x}_{k,l,f}|^2}{|\tilde{x}_{k,l,f}|_{\max}^2} \right), \quad (6)$$

where $|\tilde{x}_{k,l,f}|$ represents the amplitude of the graph signal in the joint STFT and GFT domain, $|\tilde{x}_{k,l,f}|_{\max}$ is the maximum amplitude at time-frame l , and F_N is the total number of temporal frequency bins.

Fig. 3 shows the normalized signal energy during SR along to the different graph frequencies and time, averaged over

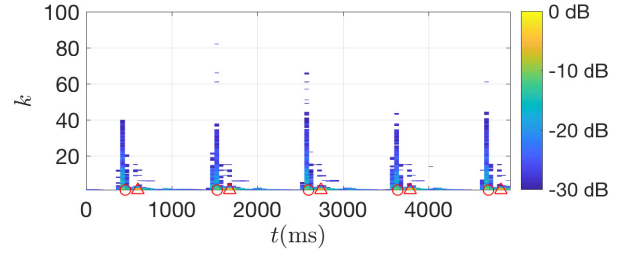


Fig. 3. Normalized energy along graph frequencies and time averaged over all temporal frequencies during SR. The red circles mark the time instants of the AA peaks and the red triangles mark the time instants of the VA peaks.

all temporal frequencies. We see that the AA presents more energy in the high graph frequencies whereas the energy of the VA concentrates itself in the low graph frequencies. Such a behavior is consistently observed over different patients. This finding suggests that the AA is more variable over the atria than the VA. Therefore, we can separate the AA and the VA in the joint domain based on their difference in the graph smoothness.

C. Atrial Activity Extraction

To extract the AA based on the graph smoothness, we first define, similar to \mathbf{X} in (4), the data matrices of the AA and the VA as \mathbf{A} and \mathbf{V} , respectively. By applying the joint STFT and GFT to the sample matrices, we can express the signal model in the joint STFT and GFT domain as

$$\tilde{\mathbf{x}}_{l,f} = \tilde{\mathbf{a}}_{l,f} + \tilde{\mathbf{v}}_{l,f} \quad (7)$$

where $\tilde{\mathbf{x}}_{l,f}$, $\tilde{\mathbf{a}}_{l,f}$, and $\tilde{\mathbf{v}}_{l,f}$ are the mixture, the AA, and the VA in the joint domain, respectively.

To quantify the spatial variation of the temporal frequency components over the graph, we consider the normalized graph Laplacian quadratic form of $\tilde{\mathbf{x}}_{l,f}$ as

$$S_n(\tilde{\mathbf{x}}_{l,f}) = \frac{\tilde{\mathbf{x}}_{l,f}^H \mathbf{L} \tilde{\mathbf{x}}_{l,f}}{\tilde{\mathbf{x}}_{l,f}^H \tilde{\mathbf{x}}_{l,f}} = \frac{\tilde{\mathbf{x}}_{l,f}^H \mathbf{\Lambda} \tilde{\mathbf{x}}_{l,f}}{\tilde{\mathbf{x}}_{l,f}^H \tilde{\mathbf{x}}_{l,f}}. \quad (8)$$

The normalization by the signal energy in (8) is done to account for the smoothness difference of the temporal frequency components obtained by the STFT.

To estimate the AA, we first estimate the VA by solving

$$\begin{aligned} & \underset{\tilde{\mathbf{v}}_{l,f}^{\text{est}}}{\text{minimize}} \quad \|\tilde{\mathbf{x}}_{l,f} - \tilde{\mathbf{v}}_{l,f}^{\text{est}}\|_2^2 \\ & \text{subject to} \quad \frac{(\tilde{\mathbf{v}}_{l,f}^{\text{est}})^H \mathbf{\Lambda} \tilde{\mathbf{v}}_{l,f}^{\text{est}}}{(\tilde{\mathbf{v}}_{l,f}^{\text{est}})^H \tilde{\mathbf{v}}_{l,f}^{\text{est}}} \leq c, \end{aligned} \quad (9)$$

where c is the normalized variation threshold for limiting the spatial variation of the reconstructed signal in the range of $[0, c]$.

The optimization problem in (9) minimizes the distortion between the mixture $\tilde{\mathbf{x}}_{l,f}$ and the estimated VA $\tilde{\mathbf{v}}_{l,f}^{\text{est}}$ in the joint STFT and GFT domain, while constraining the smoothness

of the estimated VA. To solve this problem, we rearrange it as

$$\begin{aligned} & \underset{\tilde{\mathbf{v}}_{l,f}^{\text{est}}}{\text{minimize}} \quad \|\tilde{\mathbf{x}}_{l,f} - \tilde{\mathbf{v}}_{l,f}^{\text{est}}\|_2^2 \\ & \text{subject to} \quad (\tilde{\mathbf{v}}_{l,f}^{\text{est}})^H (\mathbf{\Lambda} - c\mathbf{I}) \tilde{\mathbf{v}}_{l,f}^{\text{est}} \leq 0. \end{aligned} \quad (10)$$

By defining the Lagrangian [11]

$$L(\tilde{\mathbf{v}}_{l,f}^{\text{est}}, \lambda, c) = \|\tilde{\mathbf{x}}_{l,f} - \tilde{\mathbf{v}}_{l,f}^{\text{est}}\|_2^2 + \lambda (\tilde{\mathbf{v}}_{l,f}^{\text{est}})^H (\mathbf{\Lambda} - c\mathbf{I}) \tilde{\mathbf{v}}_{l,f}^{\text{est}} \quad (11)$$

and solving

$$\frac{\partial L(\tilde{\mathbf{v}}_{l,f}^{\text{est}}, \lambda, c)}{\partial \tilde{\mathbf{v}}_{l,f}^{\text{est}}} = \mathbf{0}, \quad (12)$$

we find the closed-form solution

$$\tilde{\mathbf{v}}_{l,f}^{\text{est}} = [(1 - \lambda c)\mathbf{I} + \lambda \mathbf{\Lambda}]^{-1} \tilde{\mathbf{x}}_{l,f}. \quad (13)$$

After estimating the VA, we subtract $\tilde{\mathbf{v}}_{l,f}^{\text{est}}$ from $\tilde{\mathbf{x}}_{l,f}$ to obtain the estimated AA $\tilde{\mathbf{a}}_{l,f}^{\text{est}}$ in the joint STFT and GFT domain per time-frame, which are then used to recover the STFT coefficients $\hat{\mathbf{a}}_{l,f}^{\text{est}}$. After obtaining the STFT coefficients of the AA in all time frames for all electrodes, the inverse STFT with overlap-adding is used to achieve the AA in the time domain for all electrodes.

IV. EXPERIMENTS AND RESULTS

We evaluate the performance of the proposed graph smoothness-based AA extraction (GAE) algorithm on synthetic and real data and compare it with the three classic algorithms including average beat subtraction (ABS) [2], adaptive ventricular cancellation (AVC) [5], and independent component analysis (ICA) [5].

A. Generation of Synthetic Data

The generation of the AA during AF is complicated since the AA and the VA typically overlap. Previous methods in [12]–[15] for simulating pure atrial electrogram work well during SR but face difficulties during AF. In this simulation, we assume that there is a atrial wave from one direction during SR whereas there are multiple atrial waves from different directions during AF. With the atrial wave being generated during SR, we can simulate its delayed versions to generate the waves from other directions. These waves are then added together to generate the pure atrial electrogram during AF.

We first synthesize the EGM during SR using the model from [14]. The ventricular segments in different heart beats in the real recording during SR are extracted out to reconstruct the pure VA. By interpolating the extracted parts with the two segments before and after them [15], we can obtain the pure atrial electrogram during SR. The ventricular electrogram obtained during SR is also used as the ventricular electrogram during AF. The pure atrial and ventricular electrograms are added to obtain the EGMs during AF. Fig. 4 shows an example of the synthetic mixture and the synthetic pure atrial electrogram at different electrodes. Atrial waves from three directions are considered in this example.

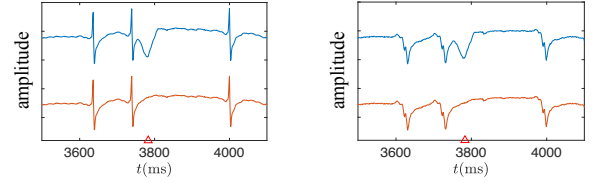


Fig. 4. An example of the synthetic mixture and the pure atrial activity at different electrodes. The blue and red curves represent the mixture and the pure atrial electrogram, respectively.

B. Performance Metrics

To quantify the performance of different algorithms, we define the normalized mean square error (NMSE) and the cross-correlation coefficient (CC) between the pure and the extracted AA. Let \mathbf{a}_{pure} and \mathbf{a}_{est} denote the pure and the estimated AA. The NMSE measures the normalized difference between the pure and the estimated AA, which is defined as

$$\text{NMSE}(\mathbf{a}_{\text{pure}}, \mathbf{a}_{\text{est}}) = \frac{\|\mathbf{a}_{\text{pure}} - \mathbf{a}_{\text{est}}\|_2^2}{\|\mathbf{a}_{\text{pure}}\|_2^2}. \quad (14)$$

The NMSE is low if the extracted AA is close to the pure AA.

The CC measures the similarity between the pure and the estimated AA. It is defined as

$$\text{CC}(\mathbf{a}_{\text{pure}}, \mathbf{a}_{\text{est}}) = \frac{(\mathbf{a}_{\text{pure}} - \mu_{\mathbf{a}_{\text{pure}}})^H (\mathbf{a}_{\text{est}} - \mu_{\mathbf{a}_{\text{est}}})}{N \sigma_{\mathbf{a}_{\text{pure}}} \sigma_{\mathbf{a}_{\text{est}}}}, \quad (15)$$

where N is the length of the signal, $\mu_{\mathbf{a}_{\text{pure}}}$ ($\mu_{\mathbf{a}_{\text{est}}}$) and $\sigma_{\mathbf{a}_{\text{pure}}}$ ($\sigma_{\mathbf{a}_{\text{est}}}$) represent the mean and standard deviation of \mathbf{a}_{pure} (\mathbf{a}_{est}), respectively. The value of CC is close to one if the pure and the estimated AA are highly correlated and zero if they are completely uncorrelated.

C. Results on Synthetic Data

We consider respectively three, four and five directions of atrial waves for generating the EGMs during AF. In each case, the EGMs are generated for 188 electrodes with a duration of 20 s each, sampled at 1 kHz. The parameters of GAE algorithm are chosen based on the grid search which minimizing the NMSE. They are set to $c = 0.14$ and $\lambda = 2$. To extract the time-frames, we apply a Hanning window with a duration of 0.1 s, taken with 50% overlap. The window length is set by the duration of the atrial and ventricular activities, which both last around 0.1 s.

Table I shows the performance during AF, including the mean and the standard deviation (in the blanket) of all electrodes. We find that the proposed method achieves the best results. ABS performs slightly worse than GAE. AVC takes the ECG as reference and its performance is not stable. It performs better than ABS when there are four sources but worse in the other two cases. ICA does not perform well as the assumptions made in this algorithm might not be applicable to the (synthetic) EGM data. GAE utilizes the recognized spatial propagation properties of the AA and the VA in the graph-time domain, which results helpful to separate the two activities.

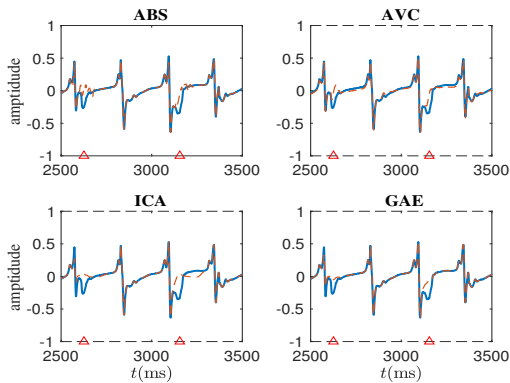


Fig. 5. Mixture (blue) at electrode 1 and extracted AA (red) by the different algorithms during AF.

TABLE I

COMPARISON OF DIFFERENT ALGORITHMS IN DIFFERENT SCENARIOS DURING AF

Scenarios	Metrics	ABS	AVC	ICA	GAE
Three sources	NMSE	0.12 (0.05)	0.18 (0.08)	0.30 (0.15)	0.10 (0.05)
	CC	0.95 (0.03)	0.92 (0.04)	0.83 (0.07)	0.96 (0.03)
Four sources	NMSE	0.10 (0.04)	0.08 (0.05)	0.22 (0.10)	0.07 (0.04)
	CC	0.95 (0.02)	0.96 (0.03)	0.82 (0.06)	0.97 (0.02)
Five sources	NMSE	0.08 (0.03)	0.11 (0.06)	0.22 (0.10)	0.05 (0.03)
	CC	0.96 (0.02)	0.95 (0.03)	0.84 (0.05)	0.98 (0.01)
Average	NMSE	0.10 (0.04)	0.12 (0.06)	0.25 (0.12)	0.08 (0.04)
	CC	0.95 (0.02)	0.94 (0.03)	0.83 (0.06)	0.97 (0.02)

D. Results on Real Data

We also conducted experiments on real data [10]. Fig. 5 and Fig. 6 show the mixture at different electrodes and the corresponding extracted AA using the different algorithms. We observe some fluctuations in the extracted signal by ABS. Furthermore, we observe that ICA cannot preserve the AA very well. In the extracted AA by AVC, there are more fluctuation and more ventricular components left than that by GAE. Compared with the other algorithms, the proposed algorithm can extract a smoother AA with less ventricular component left, which further validate the findings in Table I.

V. CONCLUSION

This work analyzed the spatial variation of the AA and the VA in EGM measurements from a new perspective by using graph-time signal processing tools. Based on the joint graph and short-time Fourier transform, we found that the frequency components of the AA is more variable over the atria than those of the VA. This finding is used to extract the AA from the mixture in the joint space-time-frequency domain. Numerical experiments on synthetic and the real data showed that the graph-smoothness based AA extraction algorithm outperforms other state-of-the-art alternatives. Future work will be on the analysis of other graph-based regularization methods to improve the performance of the atrial activity extraction algorithm.

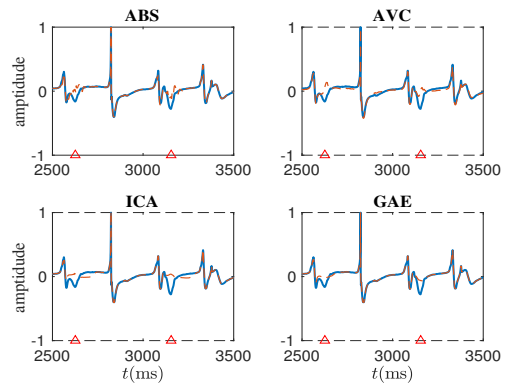


Fig. 6. Mixture (blue) at electrode 18 and extracted AA (red) by the different algorithms during AF.

REFERENCES

- [1] N. Cromie, "Atrial fibrillation," *Ulster Medical Journal*, vol. 82, no. 3, pp. 135–140, 2013.
- [2] J. Slocum, E. Byrom, L. McCarthy, A. Sahakian, and S. Swiryn, "Computer detection of atrioventricular dissociation from surface electrocardiograms during wide QRS complex tachycardias," *Circulation*, vol. 72, no. 5, pp. 1028–1036, 1985.
- [3] S. Petrutiu, J. Ng, G. M. Nijm, H. Al-Angari, S. Swiryn, and A. V. Sahakian, "Atrial fibrillation and waveform characterization," *IEEE Engineering in Medicine and Biology Magazine*, vol. 25, no. 6, pp. 24–30, 2006.
- [4] M. Lemay, J. Vesin, O. A. Van, V. Jacquemet, and L. Kappenberger, "Cancellation of ventricular activity in the ECG: evaluation of novel and existing methods," *IEEE Transactions on Biomedical Engineering*, vol. 54, no. 3, pp. 542–546, 2007.
- [5] J. J. Rieta and F. Hornero, "Comparative study of methods for ventricular activity cancellation in atrial electrograms of atrial fibrillation," *Physiological Measurement*, vol. 28, no. 8, pp. 925–936, 2007.
- [6] D. Raine, P. Langley, A. Murray, A. Dunuwille, and J. P. Bourke, "Surface atrial frequency analysis in patients with atrial fibrillation: a tool for evaluating the effects of intervention," *Journal of Cardiovascular Electrophysiology*, vol. 15, no. 9, pp. 1021–1026, 2004.
- [7] J. J. Rieta, F. Castells, C. Sánchez, V. Zarzoso, and J. Millet, "Atrial activity extraction for atrial fibrillation analysis using blind source separation," *IEEE Transactions on Biomedical Engineering*, vol. 51, no. 7, pp. 1176–1186, 2004.
- [8] A. Ortega, P. Frossard, J. Kovačević, J. M. Moura, and P. Vandergheynst, "Graph signal processing: Overview, challenges, and applications," *Proceedings of the IEEE*, vol. 106, no. 5, pp. 808–828, 2018.
- [9] D. I. Shuman, S. K. Narang, P. Frossard, A. Ortega, and P. Vandergheynst, "The emerging field of signal processing on graphs: Extending high-dimensional data analysis to networks and other irregular domains," *IEEE Signal Processing Magazine*, vol. 30, no. 3, pp. 83–98, 2013.
- [10] A. Yaksh, L. J. van der Does, C. Kik, P. Knops *et al.*, "A novel intra-operative, high-resolution atrial mapping approach," *Journal of Interventional Cardiac Electrophysiology*, vol. 44, no. 3, pp. 221–225, 2015.
- [11] S. Boyd and L. Vandenberghe, *Convex optimization*. Cambridge University Press, 2004.
- [12] J. J. Rieta, V. Zarzoso, J. Millet-Roig, R. García-Civera, and R. Ruiz-Granell, "Atrial activity extraction based on blind source separation as an alternative to QRST cancellation for atrial fibrillation analysis," in *Computers in Cardiology*, 2000, pp. 69–72.
- [13] M. Stridh and L. Sörnmo, "Spatiotemporal QRST cancellation techniques for analysis of atrial fibrillation," *IEEE Transactions on Biomedical Engineering*, vol. 48, no. 1, pp. 105–111, 2001.
- [14] F. Castells, J. Ri, J. J. Rieta, C. Sánchez, and J. Millet, "Spatiotemporal blind source separation approach to atrial activity estimation in atrial tachyarrhythmias," *IEEE Transactions on Biomedical Engineering*, vol. 52, no. 2, pp. 258–267, 2005.
- [15] F. Castells, J. Igual, J. J. Rieta, C. Sánchez, and J. Millet, "Atrial fibrillation analysis based on ICA including statistical and temporal source information," in *IEEE International Conference on Acoustics, Speech, and Signal Processing*, 2003, pp. V–94–96.